ANALYTICAL SCIENCES SEPTEMBER 2004, VOL. 20

Silica-hemin Composite Nanoparticles as New Biocatalyst to Highly Sensitive Determination of Glucose in Human Serum

Wei YANG, Hong ZHENG, Wen-Tao YUAN, and Jin-Gou XU†

The Key Laboratory of Analytical Science of MOE, Department of Chemistry, Xiamen University, Xiamen 361005, P. R. China

The preparation and utilization of a novel composite silica-hemin nanoparticles (CSHNs) as mimetic peroxidase are reported in this article. Experimental results showed that the composite nanoparticles had unique advantages over free hemin molecules in good stability and highly catalytic activity. By employing these nanoparticles as biocatalyst, we developed a new spectrofluorometric method for the determination of trace level glucose. The calibration graph for glucose was linear over the range 4.0×10^{-7} mol/L – 7.0×10^{-5} mol/L, with a detection limit of 1.0×10^{-7} mol/L. The proposed method has been successfully applied to the determination of glucose in serum samples and offers the advantages of being rapid, stable, sensitive, and renewable.

(Received April 14, 2004; Accepted June 16, 2004)

Introduction

Developing highly sensitive, nonisotopic analysis systems for biological applications has been of great importance in the fields of chemistry, biology and medical science. Because of high sensitivity and selectivity, the analytical methods based on enzymatic reactions have been widely applied.[1-3] Nevertheless, the intrinsic limitations of natural enzymes, such as instability and high cost, are still a difficult problem to be solved. So the study on mimetic enzymes becomes quite attractive.[4-9] Since the existing mimetic enzymes display lower activity compared with natural enzymes, it is highly desirable to develop new mimetic enzymes or to further enhance the activity of existing mimetic enzymes.

On the other hand, the combination of nanotechnology with analytical chemistry is a newly emerging field that has already exhibited its potential to cover practically all domains of analytical chemistry and has become an important direction for the future.[10-14] There is no doubt that the applications of nanotechnology in analytical chemistry will continue in the future because of both technological and scientific factors. Hence, in this work, we try to find a viable way to enhance the catalytic activity of mimic enzymes by integrating mimic enzymes with nanotechnology.

During the past twenty years, studies performed on organically modified silica materials prepared through the sol-gel process have been concerned about the versatility and flexibility of the preparation method.[15-18] In addition, the mild synthetic conditions offered by the sol-gel process allow the mixing of inorganic and organic components at the nanometer scale. Their ease of processing, along with several inherent advantages of sol-gel materials, such as transparency, tenability of physical properties, high photochemical and thermal stability, chemical inertness, and negligible swelling both in aqueous and organic solvents, has resulted in various applications of these nanocomposite materials.[16] Moreover, immobilization by chemical bonding is more appropriate for analytical applications. For example, it prevents the leaching of molecules and provides a more homogeneous and well-defined distribution of the organic molecules in the silica matrices, thus improving the response performance.[15]

The microemulsion route has been found to be an easy and efficient method for the preparation of nanoparticles over other existing methodologies.[19-21] Therefore, the combination of the microemulsion route with the sol-gel process is expected to be a fascinating method for preparation of various functionalized nanoparticles with tailor-made structures. Using the co-hydrolysis technique of organosilane with tetraalkoxysilicate in water-in-oil (W/O) microemulsion, a wide range of hybrid silica nanoparticles with organic modifications can be developed.[22-26] In an effort to prepare efficient and uniform nanobiocatalyst, we developed hemin-doped silica nanoparticles through covalent binding *via* W/O microemulsion method and co-hydrolysis sol-gel technique.

Hemin is a Fe-porphyrin complex; it is an inexpensive product obtained from bovine blood and exhibits some peroxidase activity.[9] In the presence of EDC, hemin reacted with 3-aminopropyltrimethoxysilane (APTMOS) to form the hemin siliylated precursor, as shown in Fig. 1. The controlled co-hydrolysis of hemin functionalized precursor and tetramethyl orthosilicate (TMOS) in W/O microemulsion led to the formation of mono-dispersed CSHNs. The properties of the nanoparticles were also investigated. The present work shows that the CSHNs have higher catalytic activity than free hemin and that the incorporated technique described above is promising for improving the catalytic activity of mimic enzymes.

Thus, a new spectrofluorometric method using the composite silica-hemin nanoparticles as the catalyst was developed for the sensitive determination of trace level glucose. The calibration

† To whom correspondence should be addressed.
E-mail: jgxu@xmu.edu.cn

graph for glucose was linear over the range of 4.0×10^{-7} – 7.0×10^{-5} mol/L, with a detection limit of 1.0×10^{-7} mol/L. And the proposed method has been successfully applied to the determination of glucose in serum samples with the advantages of being rapid, stable, sensitive, and renewable.

Experimental

Materials

Triton X-100 and hemin were purchased from Acros; *p*-hydroxyphenylacetic acid (*p*-HPA), 3-aminopropyltrimethoxysilane (APTMOS) and tetramethyl orthosilicate (TMOS) were obtained from Aldrich; ethyl-[3-(dimethylamino)propyl]carbodiimide hydrochloride (EDC), glucose oxidase (GOD) (high pure, 111 U/mg) and β-D-glucose were purchased from Sigma. All other regents were of analytical grade. The concentration of hydrogen peroxide (H_2O_2) was standardized by titration with secondary standard potassium permanganate. Samples of sera were donated by the Hospital of Xiamen University and used directly without further preparations. A Millipore Milli-Q system provided water for all experiments.

Apparatus

The steady-state fluorescence spectra were recorded on a Hitachi F-4500 spectrofluorimeter. UV-Vis absorption spectra were recorded on a Beckman DU-7400 UV-VIS diode array spectrophotometer. Transmission electron microscopy (TEM) micrographs of the particles were obtained from a JEOL JEM-100CXII (100 kV) transmission electron microscope. Each ESI mass spectrum was recorded on a Finnigan MAT LCQ ESI mass spectrometer. Confocal Resonance Raman Spectroscopy (RRS) was carried out on a Renishaw UV-Visible R1000 system with excitation at 514.5 nm provided by an argon ion laser.

Synthesis of hemin-functionalized precursor

To a 2 mL aliquot of anhydrous dimethylformamide (DMF), 50 mg hemin was added. The mixture was stirred for 5 min to achieve complete dissolution of hemin, then 30 mg EDC was added with stirring for another 5 min. Finally, 20 µL APTMOS was added to the mixture and mixed in well. The reaction was conducted for 20 h with stirring under room temperature (about 15˚C), and the product, hemin-functionalized precursor, was collected. The product was first tested by thin layer chromatography (TLC) (SiO_2; CH_3CN), and then characterized by mass spectrometry.

Synthesis of composite SiO_2-hemin nanoparticles

A W/O reverse microemulsion was prepared with nonionic surfactant Triton X-100 by using a procedure similar to that described by Jain.[24] The microemulsion was prepared at ambient temperature, typically consisting of 10.6 mL Triton X-100, 25 mL cyclohexane, 10.8 mL hexanol and 2.25 mL H_2O. The final mixture formed a clear solution. After stirring for 10 – 15 min, 0.8 mL neat TMOS was added drop by drop to the microemulsion and the mixture was stirred vigorously for 10 – 15 min to impel TMOS diffused into the aqueous core of reverse microemulsion droplets. An appropriate amount of hemin functionalized silica precursor was slowly added into the mixture; 0.8 mL NH_4OH (25%) was then added to initiate the hydrolysis. The reaction was allowed to continue for 24 h to ensure completion of the condensation.

After the reaction was completed, the materials prepared in the reverse microemulsion could be recovered by roto-evaporation at 30˚C. Then the nanoparticles were isolated by acetone, followed by centrifuging and washing with ethanol and water several times to remove any surfactant molecules.[26] We used ultrasonication while washing the nanoparticles to remove any physically adsorbed surfactant molecule from the particles. The particles were then dried in a vacuum for over 20 h at 30˚C. The size and morphology of the composite nanoparticles dispersed were characterized by TEM.

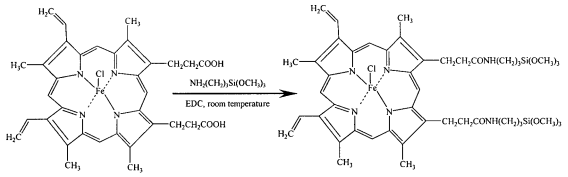

Fig. 1 Synthesis of hemin functionalized precursor.

Characterization of composite nanoparticles by UV-Vis absorption spectrum

An appropriate amount of composite nanoparticles was dispersed into 5 mL NH_3–NH_4Cl buffer solution (pH = 10.0). The absorption spectra were recorded after 5 min ultrasonication of the solution. And the amount of bound hemin was determined by UV-Vis absorption spectrum according to reference.[27] To determine the content of hemin in composite particles, we dissolved the particles in NaOH solution and we measured the UV-Vis spectrum of the obtained solution. For this purpose, to an accurately weighed amount (~25 mg) of nanoparticles was added 10 mL of 0.25 mol/L NaOH and the dispersion was left standing for ~4 h, resulting in complete dissolution of the solid. Then, a series of solutions of free hemin in 0.25 mol/L NaOH were prepared and their UV-Vis spectra were measured to get a calibration curve. This calibration curve was then used to determine the content of hemin in the composite nanoparticles.

Characterization of composite nanoparticles by confocal resonance Raman spectroscopy (RRS)

Samples were prepared according to the literature.[28] An appropriate amount of samples (with the same concentration of hemin) was dispersed into 1 mL of the ethanol–water (v:v = 2:1) mixture and the solution then pipetted onto a glass slide. After the solution was vaporized, the laser was then positioned onto a specific point of the sample and spectra were detected. The sampling time was limited to 200 s. The spectral resolution was ~2 cm^{-1}. Each spectrum was obtained from six different points on four separately prepared samples.

Determination of activities of immobilized hemin

For assessment of the overall enzymatic reaction performance, the well-known reaction of nonfluorescent *p*-HPA with H_2O_2 was used, forming the fluorescent product, 2,2′-dihydroxy-diphenyl-5,5′-diacetic acid.[29]

Kinetic experiments to investigate the catalytic behavior as a function of reaction time were conducted by mixing 5.0×10^{-6} mol/L CSHNs (or free hemin) with 5.0×10^{-6} mol/L of H_2O_2 and *p*-HPA (2.0×10^{-6} mol/L) at pH 10.0 (0.05 mol/L NH_3–NH_4Cl) at room temperature. The catalytic activity of silica-hemin nanoparticles (5.0×10^{-7} mol/L, in 0.05 mol/L NH_3–NH_4Cl, *p*H = 10.0) in the reaction of *p*-HPA and H_2O_2 was studied by the initial-rate method. Here, one makes the

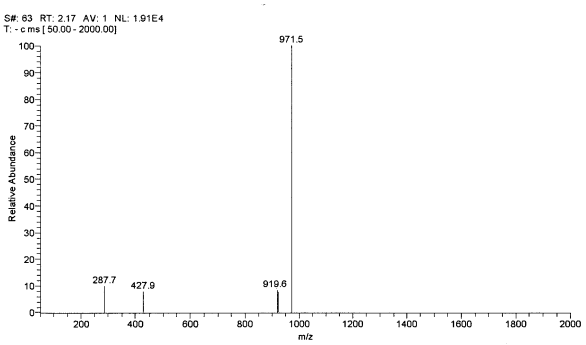

Fig. 2 MS spectrum of hemin functionalized precursor.

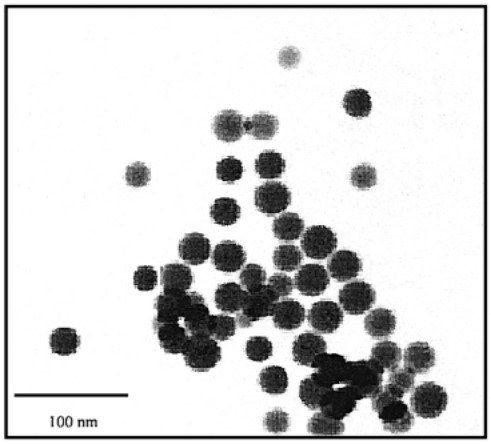

Fig. 3 TEM image of SiO_2-hemin composite nanoparticles.

concentration of one of the substrates constant and in great excess; then the mimetic peroxidase catalyzed process is a quasi-first order reaction, and Michaelis–Menten behavior is observed. In the test system, the concentration of H_2O_2 was saturated and the concentration of *p*-HPA was changeable from 5.0×10^{-7} mol/L to 3.0×10^{-5} mol/L.

Determination of glucose in human serum

Glucose can produce H_2O_2 under the action of GOD; thus it can be indirectly measured by the determination of H_2O_2. The procedure is as follows: In a 10 mL volumetric flask, a series of glucose solutions, 0.5 mL of 2.0 U/mL GOD and 0.5 mL of phosphate buffer solution (pH 7.0) were added. After incubation for 5 min under 25°C, the mixture was cooled down immediately to 0°C to stop the oxidation reaction. Then, to the above mixture, 2.0 mL of a solution containing CSHNs (2.0×10^{-5} mol/L, NH_3–NH_4Cl buffer, pH = 10.0), 1.0 mL of *p*-HPA (2.0×10^{-6} mol/L) were introduced and diluted with water to the mark.

The relative fluorescence intensity of the product was subsequently measured at 420 nm with excitation at 320 nm after 15 min under room temperature. The excitation and emission band-passes were both set at 10 nm. The calibration curve was then constructed by plotting the relative fluorescence intensity *vs*. glucose concentration. Real serum samples were manually diluted with water and analyzed as described above.

Results and Discussion

Synthesis of hemin-functionalized precursor

In the presence of EDC, APTMOS can be modified by hemin *via* the formation of amido bond to obtain the hemin-functionalized precursor (Fig. 1). Since methoxysilane groups may be hydrolyzed during the purification and isolation processes of functionalized monomer, hemin and APTMOS were strictly kept in a 1:2 molar ratio for a stoichiometric reaction in order to avoid the isolation and purification of the monomer. Solvents used must be anhydrous. The reaction process was monitored by TLC (SiO_2; CH_3CN). The product was characterized by mass spectrometry. The mass spectrum of the monomer exhibited an intense signal at *m/z* 971.5 corresponding to [hemin-bis(propyltrimethoxysilane)]$^+$ (Fig. 2). No signals corresponding to hemin or APTMOS species were observed.

Synthesis of composite nanoparticles

The reverse microemulsion route was used to prepare the composite nanoparticles. By the co-hydrolysis of organosilane with tetraalkoxysilicate in reverse microemulsion system, discrete spherical composite silica-hemin nanoparticles were obtained. The TEM photograph showed that the particles were uniform and monodispersed with a diameter of about 30 ± 5 nm, and hemin was dispersed homogeneously throughout the silica network (Fig. 3). Further experiments showed that no hemin molecules could be washed out from the nanoparticles, either with hot water or by extraction with hot ethanol for several days, which indicated that the anchored amido bonds are adequately stable. In contrast, hemin molecules without anchored groups were easily removed within a few minutes.

To tailor the particle size, morphology and structure of the nanoparticles, we carefully controlled the synthesis parameters such as the composition of the reverse microemulsion, the ratio of water to alkoxide, the aging time, the powder recovery and the drying technique. The size of the nanoparticles was primarily controlled by the molar ratio of water to surfactant (*R*) and the molar ratio of water to TMOS (*H*); as the values of *R* and *H* increased, the particle size was decreased.[23] The TEM micrographs showed that the size of composite particles changed linearly with *R* and *H* from 30 nm to 80 nm.

Particle growth may be minimized by short reaction time. However, appropriate aging time is essential to ensure completion of the condensation reaction. Condensation of the surface hydroxyl groups led to particles that were less susceptible to agglomeration in subsequent reaction.[23] We determined that the optimal reaction period for our system was 20 – 24 h.

UV-Vis spectral characterization

As shown in Fig. 4, the absorption spectra for the pure hemin and composite SiO_2-hemin nanoparticles displayed almost the same profile in aqueous solution (0.05 mol/L NH_3–NH_4Cl buffer, pH = 10.0), which implies that the structure of hemin molecules in the composite nanoparticles is well retained. Hemin has good solubility in NaOH aqueous solution[9] and its concentration can be determined by UV-Vis spectrophotometry. The calibration curve showed a linear relationship between the absorbance and the concentration of hemin over the range of 4.0×10^{-6} mol/L to 6.0×10^{-4} mol/L. The content of hemin in the nanoparticles was determined by UV-Vis spectrophotometry after the material was dissolved in NaOH solution. In light of the above results and in a rough estimation, those composite particles can achieve a high hemin loading of about 36 mg/g (5.52×10^{-5} mol/g). We then employed these nanoparticles as

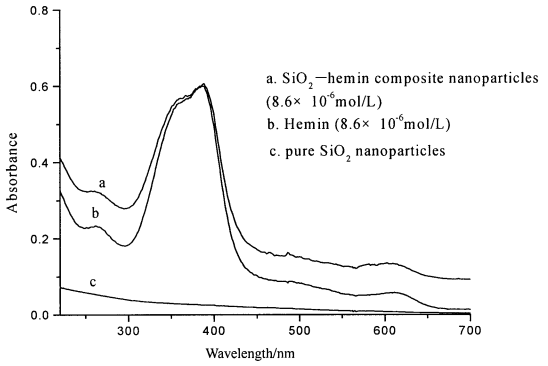

Fig. 4 UV-Vis spectra of SiO_2-hemin composite nanoparticles.

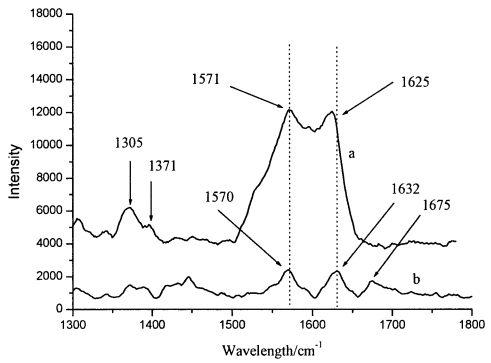

Fig. 5 RRS spectra of SiO_2-hemin composite nanoparticles. a, SiO_2-hemin composite nanoparticles; b, free hemin.

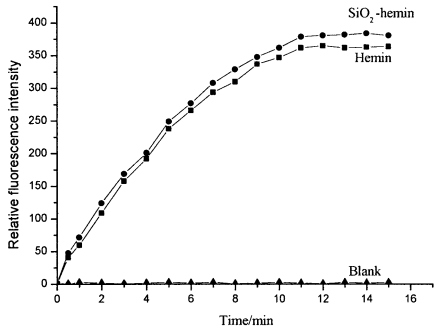

Fig. 6 Catalytic behavior of SiO_2-hemin composite nanoparticles.

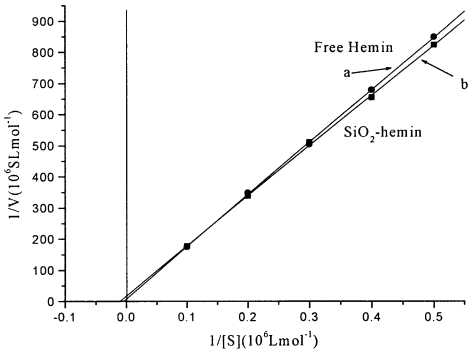

Fig. 7 Lineweaver–Burk plot.

the catalyst in further experiments.

Structural analysis of immobilized hemin by resonance Raman spectrum (RRS)

For the molecules containing heme groups, RRS is a more informative structural probe than FT-IR as it provides detailed information that is not possible to obtain by FT-IR.[27] The prominent vibrational bands in the RRS of hemin are the result of a vibronic coupling mechanism. The presence of in-plane ring modes in such molecules, which are coupled with π-π* excitation, allows the selectively strongly enhanced Raman bands to be detected when such bands are in resonance with any of the dominant electronic transitions.[28,30-34] These bands have been extensively correlated with particular heme vibrational modes.[30-34] It has been shown that bands above 1300 cm^{-1} correlate with structural parameters of the heme environment such as oxidation and spin states as well as with the coordination numbers of the heme iron.[28,30-34] These refer largely to nontotally symmetric vibrations, the most distinct of which are the spin-state marker bands.[28] RRS of hemin in aqueous solution and 30 nm composite nanoparticles are shown in Fig. 5. The spectra acquired at different positions on the same sample were the same, suggesting that the environment for hemin in nanoparticles was similar.

It can be seen that the spectrum obtained with hemin incorporated in 30 nm composite nanoparticles is quite different from that obtained with free hemin. The intensity ratio of bands around 1600 cm^{-1} to bands around 1300 cm^{-1} of the former is larger than that of the latter, which indicates that hemin molecules incorporated in the composite nanoparticles undergo some structural changes compared to free hemin in aqueous solution. Moreover, it can also be seen that the peak at 1625 cm^{-1} for hemin incorporated in 30 nm composite nanoparticles has a 7 cm^{-1} shift compared with the peak at 1632 cm^{-1} for free hemin in aqueous solution. This means that most of the hemin molecules in nanoparticles exist in higher spin states, leading to higher catalytic activity.[28] The phenomenon observed with silica-hemin nanoparticles, *i.e.* most of heme Fe being in high spin state, is attributed to the interaction between hemin and nanoparticles. Under room temperature, however, free hemin is predominantly in a low spin state with an RRS band at 1632 cm^{-1}.[28] In the spectra, the dimer of hemin molecules was not observed.

Determination of activities of immobilized hemin

The hemin-catalyzed reaction of *p*-HPA with H_2O_2 was used to examine the catalytic kinetics of the immobilized hemin and free hemin, the results are shown in Fig. 6. It can be seen that their kinetic behaviors are similar. The kinetics of the immobilized hemin observed in this study follows the Michaelis–Menten mechanism. The relationship between the reaction rate and the concentration of substrate can be expressed by the following equation: $1/v = (k_m/V_{max})\cdot 1/[S]+1/V_{max}$, where v and V_{max} denote the initial reaction rate and the maximum reaction rate, respectively, k_m is the Michaelis constant, and [S] denotes the concentration of substrate. The values of v at different concentrations of substrate, [S], were measured, then a Lineweaver–Burk graph ($1/v$ *versus* 1/[S]) was plotted (Fig. 7). From the Lineweaver–Burk graph, the values of k_m and V_{max} were obtained. Since $V_{max} = K_{cat}[E_0]$, where K_{cat} denotes the turnover rate and $[E_0]$ denotes the concentration of enzyme, the value of K_{cat}, which indicates the activity of enzyme, can be obtained when the values of V_{max} and $[E_0]$ are known. The greater the value of K_{cat}, the greater the activity will be. The

Table 1 Catalytic parameters with SiO_2-hemin composite nanoparticles or free hemin as a catalyst and *p*-HPA as a substrate

Catalyst	K_m (10^{-6} mol/L)	V_{max} (10^{-6} mol/Ls)	$[E_0]$ (10^{-8} mol/L)	K_{cat} (s^{-1})
Free hemin	89.4	0.06	5	1.1
SiO_2-hemin	202.3	0.12	5	2.3

bulk solution value was measured using the same Lineweaver–Burk analysis. Catalytic parameters obtained from the Lineweaver–Burk plot are listed in Table 1. From Table 1 it can be seen that the activity of hemin incorporated in composite nanoparticles is twice the activity of free hemin.

The enhancement of mimetic enzyme activity is attributed to the influence of the nanostructure. We speculate that the nanostructures provided the hemin molecules with a benign surrounding microenvironment, showing higher substrate affinity for hemin molecules. Moreover, the immobilization prevents hemin molecules from aggregation, and the nanostructures increase the accessibility of active sites to the substrate due to the increase of effective surface. On the other hand, the higher activity may originate from the fast interaction between immobilized hemin and substrate molecules in solution, owing to the high spin state as described above, *i.e.* faster charge transfer is achieved. Moreover, the nanostructures may induce the quite order orientations of hemin molecules and their interactions were enhanced with each other closed packed. However, it is still necessary to do more detailed experiments to fully establish the mechanism for the interaction between hemin and nanoparticles.

Stabilities of immobilized hemin

Usually, native enzyme quickly loses activity; therefore, storage stability, thermostability and operational stability are important factors for the applicability of immobilized biocatalyst.

After the hemin incorporated in nanoparticles was stored at 4˚C for 60 days, its activity decreased to 98% of its initial activity. However, free hemin in solution only retained 84% of its initial activity under the same condition. After storage for 60 days at room temperature, the activity of free hemin in solution reduced 74%, but the activity of hemin incorporated in nanoparticles decreased only 12%. When treated in water at 70˚C for 30 min, free hemin lost more than 60% of its initial activity, but hemin immobilized in nanoparticles only lost 30% of its initial activity. The operational stability was tested by continuously measuring the activity of the silica-hemin nanoparticles recycled *via* simple washing with water by ultrasonication and collection by centrifugation. The primary tests conducted were 6 cycles. The activity retained 94% – 96% of initial activity. We think that the composite nanoparticles can be used for more cycles.

The above results show that the hemin incorporated in silica nanoparticles can be used over a wider temperature range, which may contribute to the functionalized nanostructures; the hemin molecules doped inside the silica nanostructures get well protected from the surrounding environments.

Interference effects of various compounds on the assay of glucose

The interference of common foreign substances with the determination of glucose (1.0×10^{-5} mol/L) was examined; the results are summarized in Table 2. When a relative error of less than ±5% is required, it can be seen that among common metal ions, only Pb^{2+}, Fe^{3+} and Cu^{2+} cause little interference. It was also observed that the interference of those cations could be eliminated in the presence of suitable amounts of EDTA, since EDTA formed stable complexes with those metal ions. However, when the system is used for the determination of glucose in serum, the sample is highly diluted, which largely decreases the levels of metal ions and thus eliminates their interference. Therefore, it is not necessary to add EDTA in this case. Furthermore, the concentrations of bilirubin and hemoglobin in human serum are low enough to be ignored. Furthermore, vitamin C at normal level in serum samples does not affect the assay yet.

Table 2 Tolerance of foreign substances in the determination of glucose (1.0×10^{-5} mol/L)

Interfering species	Tolerance (molar ratios)	Interfering species	Tolerance (molar ratios)
Na^+, K^+, Cl^-, NH_4^+, CO_3^{2-}	5000	Zn^{2+}, Mg^{2+}	100.0
Al^{3+}	100	Ba^{2+}	500
NO_3^-	2000	Pb^{2+}, Cu^{2+}, Mn^{2+}	20
Ni^+, Ca^{2+}	100	Glycine,	250
NO_2^-, CH_3COO^-	500	Bilirubin	1.0
Hemoglobin	2.5	Triglyceride	50
Tyrosine	50	Alanine	100
Maltose	100	Sucrose	100
Fructose	100	Citric acid	200

Table 3 Determination of glucose in fresh human sera

Sample	Concentration of glucose (10^{-3} mol/L)		Added (10^{-7} mol/L)	Found (10^{-7} mol/L)	Rec., %	RSD, % ($n = 6$)
	Enzyme kit[a]	Proposed method[b]				
1	5.20	5.10	3.00	2.96	98.7	3.4
2	5.55	5.48	3.00	2.88	96.0	2.8
3	6.80	6.92	3.00	3.06	102.0	2.1

a. These data were provided by the hospital using an enzyme kit.
b. Mean of six determinations.

Determination of glucose in human serum

Glucose is important in the bioanalytical science for a number of reasons.[35,36] GOD and glucose are still of great importance as analyte recognition systems in biosensors.[35,36] Each system was optimized to various working parameters. The impact of various buffers on the catalytic reaction system was examined, and the results showed that the activity of these composite nanoparticles in NH_3–NH_4Cl medium was higher than that in other buffers. Therefore, NH_3–NH_4Cl (0.05 mol/L, pH = 10.0) buffer was recommended for use. And this acidity is also satisfactory for the development of fluorescence. When the concentration of *p*-HPA was varied from 1.0×10^{-6} – 3.0×10^{-6} mol/L, the fluorescence was maximum and constant, hence 2.0×10^{-6} mol/L of *p*-HPA was employed in the subsequent work. The fluorescence intensity was maximum when the concentration of silica-hemin nanoparticles varied from 1.5×10^{-5} – 4.0×10^{-5} mol/L, therefore, a concentration of 2.0×10^{-5} mol/L was adopted in the standard procedure for rapid assay of glucose. The calibration graph for glucose was linear over the range of 4.0×10^{-7} – 7.0×10^{-5} mol/L, with a detection limit of

1.0×10^{-7} mol/L (LOD = $3\sigma/S$, n = 20). The regression equation is $\Delta F = 15.84C(10^{-6}$ mol/L) + 0.41, with a correlation coefficient of 0.9992. The relative standard deviation was 2.6% (n = 10) for the determination of glucose (1.0×10^{-6} mol/L).

The samples were also analyzed in a hospital laboratory by an Enzyme Kit method. As listed in Table 3, no marked difference is found. The accuracy and reliability of the method was investigated by performing the recovery tests of standard addition in real sample. The recovery experiments gave satisfactory results of 96.0 – 102.0% with a < 4% relative standard deviation (n = 6).

Conclusion

Novel, uniform and stable composite silica nanoparticles encapsulating hemin through covalent bond have been prepared and characterized for the first time. Because of the tiny size and high functionality, they can be uniformly dispersed in water and behave like single dissolved molecules to form a transparent colloidal solution; especially, these materials are transparent to visible light. The properties of immobilized hemin, such as the catalytic activity, stability and recycle, were studied. The silica-hemin composite nanoparticles showed high immobilization efficiency and stability of hemin, and the high affinity to the substrate molecules, leading to higher catalytic activity and stability over the free hemin in aqueous solution.

In this paper, the applicability of the composite nanoparticles as a catalyst was demonstrated in the system for the detection of trace level glucose. The sensitivity of the proposed system was notably increased compared with the corresponding system using free hemin as a catalyst. We think the covalent binding of a mimetic enzyme to silica nanoparticles described in this study is a powerful tool for optimizing the properties of the mimetic enzyme, and this approach has good prospects for potential applications.

References

1. T. Neufeld, A. Schwartz-Mittelmann, D. Biran, E. Z. Ron, and J. Rishpon, *Anal. Chem*., **2003**, *75*, 580.
2. D. Xiao and M. M. F. Choi, *Anal. Chem*., **2002**, *74*, 863.
3. A. K. Williams and J. T. Hupp, *J. Am. Chem. Soc*., **1998**, *120*, 4366.
4. L. H. Chen, L. Z. Liu, and H. X. Shen, *Anal. Chim. Acta*, **2003**, *480*, 143.
5. H. H. Yang, Q. Z. Zhu, D. H. Li, L. X. Chen, M. T. Ding, and J. G. Xu, *Anal. Chim. Acta*, **2001**, *435*, 265.
6. M. C. Feiters, A. E. Rowan, and R. J. M. Nolte, *Chem. Soc. Rev*., **2000**, *29*, 375.
7. T. G. Back and B. P. Dyck, *J. Am. Chem. Soc*., **1997**, *119*, 2079.
8. B. Tang, G. Y. Zhang, Y. Liu, and F. Han, *Anal. Chim. Acta*, **2002**, *459*, 83.
9. Q. Z. Zhu, F. H. Liu, D. H. Li, J. G. Xu, W. J. Su, and J. W. Huang, *Anal. Chim. Acta*, **1998**, *375*, 177.
10. C. M. Niemeyer, *Angew. Chem. Int. Edit*., **2001**, *40*, 4128.
11. D. W. Deamer and D. Branton, *Accounts Chem. Res*., **2002**, *35*, 817.
12. Z. Y. Zhong, K. B. Male, and J. H. T. Luong, *Anal. Lett*., **2003**, *36*, 3097.
13. D. M. Willard, *Anal. Bioanal. Chem*., **2003**, *376*, 284.
14. I. Willner and B. Willner, *Pure Appl. Chem*., **2002**, *74*, 1773.
15. M. M. Collinson, *TrAC*, *Trends Anal. Chem*., **2002**, *21*, 30.
16. C. Sanchez, B. Lebeau, F. Chaput, and J. P. Boilot, *Adv. Mater*., **2003**, *15*, 1969.
17. M. M. Collinson, *Crit. Rev. Anal. Chem*., **1999**, *29(4)*, 289.
18. R. A. Caruso, *Chem. Mat*., **2001**, *13*, 3272.
19. J. Klier, C. J. Tucker, T. H. Kalantar, and D. P. Green, *Adv. Mater*., **2000**, *12*, 1751.
20. M. A. Lopez-Quintela, *Curr. Opin. Colloid Interface Sci*., **2003**, *8*, 137.
21. S. Vaucher, M. Li, and S. Mann, *Angew. Chem. Int. Ed*., **2000**, *39*, 1793.
22. X. J. Zhao, R. P. Bagwe, and W. H. Tan, *Adv. Mater*., **2004**, *16*, 173.
23. A. J. Zarur and J. Y. Ying, *Nature*, **2000**, *403*, 65.
24. T. K. Jain, I. Roy, and T. K. De, *J. Am. Chem. Soc*., **1998**, *120*, 11092.
25. J. Esquena, T. F. Tadros, K. Kostarelos, and C. Solans, *Langmuir*, **1997**, *13*, 6400.
26. W. Yang, C. G. Zhang, H. Y. Qu, H. H. Yang, and J. G. Xu, *Anal. Chim. Acta*, **2004**, *503*, 163.
27. M. Bele, O. Siiman, and E. Matijevic, *J. Colloid Interface Sci*., **2002**, *254(2)*, 274.
28. J. Deere, E. Magner, J. G. Wall, and B. K. Hodnett, *J. Phys. Chem. B*, **2002**, *106(29)*, 7340.
29. M. Heule, K. Rezwan, L. Cavalli, and L. J. Gauckler, *Adv. Mater*., **2003**, *15*, 1191.
30. C. Colas and P. R. O. de Montellano, *Chem. Rev*., **2003**, *103*, 2305.
31. H. M. Marques and K. L. Brown, *Coord. Chem. Rev*., **2002**, *225*, 123.
32. T. G. Spiro, M. Z. Zgierski, and P. M. Kozlowski, *Coord. Chem. Rev*., **2001**, *219*, 923.
33. L. M. Proniewicz and J. R. Kincaid, *Coord. Chem. Rev*., **1997**, *161*, 81.
34. P. Hildebrandt and P. M. Stockburger, *J. Phys. Chem. B*, **1986**, *90*, 6017.
35. M. Morikawa, N. Kimizuka, M. Yoshihara, and T. Endo, *Chem.—Eur. J*., **2002**, *8*, 5580.
36. N. Piza, M. Miro, J. M. Estela, and V. Cerda, *Anal. Chem*., **2004**, *76*, 773.